Conformational Changes and Catalytic Competency of Hydrolases Adsorbing on Fumed Silica Nanoparticles: I. Tertiary Structure

Juan C. Cruz[1], Peter H. Pfromm[1]*, John M. Tomich[2], Mary E. Rezac[1]

(1) Department of Chemical Engineering, Kansas State University, 1005 Durland Hall, Manhattan, KS 66506 - 5106, USA.

(2) Department of Biochemistry and Biotechnology/Proteomics Core Facility, Kansas State University, Burt Hall, Manhattan, KS 66506 - 5106, USA.

Please cite this article as: J.C. Cruz et al., Conformational changes and catalytic competency of hydrolases adsorbing on fumed silica nanoparticles: I. Tertiary structure, *Colloids Surf. B. Biointerfaces* 79 (2010), 97-104.

Abstract

We have recently introduced an immobilization protocol for preparations of enzymes on fumed silica for catalysis in organic solvents. The observation of a maximum in apparent catalytic activity at intermediate surface coverage for one enzyme while another enzyme showed continuously increasing apparent catalytic activity with decreasing surface coverage led to speculation on the impact of surface coverage on apparent catalytic activity through different relative surface-protein and protein-protein interactions, combined with different "hardness" or resistance towards unfolding by the enzymes. The kinetics of tertiary unfolding of *Candida antarctica* Lipase B (CALB), *subtilisin Carlsberg*, and the Lipase from *Thermomyces lanuginosus* (TLL) adsorbing on fumed silica nanoparticles were inferred here from tryptophan fluorescence for 2%SC to 1250%SC, 0.5 mg/mL to 4.70 mg/mL enzyme concentration in aqueous buffer solution, and in the presence of the structural modifiers 2,2,2-trifluoroethanol (TFE) and Dithiothreitol (DTT). The results shown here confirm the earlier speculation that "hard" enzymes can perform well at low and intermediate surface coverage of the solid fumed silica particles until multi-layer packing imposes mass transfer limitations, while "soft" enzymes unfold at low surface coverage and therefore show a maximum in catalytic competency at intermediate surface coverage before declining apparent activity is caused by multi-layer packing.

Keywords: Conformational Stability; Adsorption; Fumed Silica; CALB; TFE; DTT.

*Corresponding author: Tel: +1 785 532 4312; fax: +1 785 532 7372

E-mail address: pfromm@ksu.edu

Introduction

The synthesis of organic compounds often requires non-aqueous media due to solubility and stability issues, and undesirable side reactions in the presence of water [1-7]. Many chemical synthesis schemes require multiple steps and may involve toxic inorganic catalysts as well as generate undesirable by-products [8, 9]. One avenue to overcome the issues with chemical synthesis has been the extension of enzymatic catalysis in aqueous media to non-aqueous media exploiting the exquisite regio- and stereo- selectivity of enzymes [2, 5, 10] in addition to the fact that enzymatic catalysts are generally renewable and non-toxic. However, poor enzyme solubility in solvents [11] generally requires to either solubilize the enzyme or immobilize it on a solid support [12-18] to avoid mass transfer limitations for the desired reaction. There has been an increasing interest in the immobilization of enzymes on nanoparticles due to their unique properties including the extremely large surface area per mass [19].

We have recently introduced an immobilization protocol with an inexpensive nanostructured support [16-18]. Fumed silica is a fractal aggregate that consists of individual spherical non-porous nanoparticles linked in necklace-like structures [20-22]. This material has proven to be an exceptional adsorbent for proteins and polymers [23-25]. In our two-step immobilization protocol, the enzyme molecules are first physically adsorbed on fumed silica in an aqueous buffer. The adsorbate is then lyophilized. We have previously considered *subtilisin Carlsberg* and *Candida antarctica* Lipase B (CALB) to assess our immobilization protocol, alterations in physical properties, and the impact on the catalytic competency. These enzymes were chosen due to their wide range of applications in nonaqueous media. The maximum observed catalytic activity in hexane reached or even exceeded commercial immobilizates of CALB [13-15] and what has been termed "salt-activated" preparations for *s. Carlsberg* [26, 27]. CALB is a monomeric 317 residue protein [28] with five tryptophan (Trp52, Trp65, Trp104, Trp113 and Trp155) nine tyrosine, and ten phenylalanine residues, which can be monitored to follow conformational changes [28]. CALB's structure is stabilized by four disulfide bridges [28]. The *s. Carlsberg* protein is a single polypeptide chain consisting of 274 amino acid residues [29] including one surface exposed tryptophan (Trp117) and thirteen tyrosine residues [30, 31]. The Trp fluorescence of *s. Carlsberg*, however, dominates mainly due to quenching and energy transfer mechanisms [30, 31].

We have previously reported on the relationship of surface coverage to apparent catalytic activity of enzymes immobilized on fumed silica [16-18]. The *s. Carlsberg* exhibited a constant increase in apparent catalytic activity as more surface area is provided per enzyme molecule for immobilization. This enzyme increase levels off after sufficient area is available for a nominally "sparse" surface population. CALB, however, showed a maximum in apparent catalytic activity with steep decreases at both higher and lower surface coverage. In accordance with previously reported observations [12-15], we postulated that this maximum in apparent catalytic activity corresponds to a surface loading regime at intermediate surface coverage that results from the overlapping of two other surface regimes at high and low coverages: I. low surface coverage with opportunities for multi-point attachment of the enzyme on the support promoting detrimental conformational changes, II. an intermediate surface coverage where some interactions with neighboring enzyme molecules in addition to interactions with the support surface help to maintain a higher population of catalytically competent enzyme molecules, and III. increasingly multi-layer coverage where mass transfer limitations reduce the apparent catalytic activity with increasing enzyme loading per support area.

The multi-point attachment and deformation under regime I. appears to promote substantial conformational changes and consequently loss of catalytic activity for CALB. Previous investigations have demonstrated that proteins can either deform or maintain their structure upon adsorption on nanomaterials [32-35] depending on the chemistry, size, and curvature of the nanomaterials [36], the intricate intermolecular forces between the surface and the protein [37], and the conformational stability of the protein [38, 39]. A more complete understanding of these phenomena appears crucial not only for enzyme based biocatalysis but for a number of emerging fields including nanobiophotonics [40, 41] and nanobioelectronics [42, 43].

Hitherto, information regarding in-situ conformation/structure of immobilized enzyme molecules remains scarce [44]. A characterization of the folding/unfolding tendencies for enzymes interacting with surfaces will help to engineer strategies for the development of structurally stable and highly active biocatalysts for use in solvents [39, 44-46]. Fourier Transform Infrared- (FTIR), Circular Dichroism- (CD), Intrinsic Fluorescence-, Raman optical activity- and Nuclear Magnetic Resonance (NMR) spectroscopy techniques are the preferred techniques for conformational assessment of proteins [39, 44-49]. The intrinsic tryptophan fluorescence has been described as particularly well suited for characterizing tertiary conformational changes of adsorbed proteins on nanomaterials [39, 45, 46, 50]. Fluorescence spectroscopy is applied here to probe the kinetics of tertiary conformational changes of enzymes adsorbing on fumed silica nanoparticles from the aqueous phase for CALB, *s. Carlsberg* and the Lipase from *Thermomyces lanuginosus* (TLL). TLL was added as an external control representing high intrinsic conformational stability.

We show evidence that for CALB in hexane the previously observed maximum in apparent catalytic activity, at an intermediate surface coverage of fumed silica nanoparticles, is most likely related to the low conformational stability of this enzyme. Conversely, the *s. Carlsberg* and TLL enzymes appear to be conformationally more stable. The time-course of unfolding during and after adsorption on fumed silica followed for about 40 minutes clearly shows that CALB undergoes some unfolding and refolding until a equilibrium is reached as would be expected for a "soft" enzyme [51]. Structurally "hard" *s. Carlsberg* and TLL, however, unfold gradually before reaching equilibrium on fumed silica at both low and high surface coverages. At equilibrium, all three enzymes exhibited distinctly different regions of conformational stability. Comparison with the apparent catalytic activity of the lyophilized enzyme adsorbates in hexane demonstrates that the postulated impact of changing surface coverage on the stabilization of adsorbed molecules is corroborated by the spectroscopic unfolding measurements. We will also discuss the impact of structure modifiers on the conformational stability conditions and thereby on immobilization on fumed silica.

To our knowledge the data presented here represents the first attempt to understand the impact of surface packing density changes on the conformational stability of enzymes adsorbed on fumed silica nanoparticles. Previous reports [39, 45, 46] have considered colloidal silica nanoparticles which have bigger hydration layers and narrower particle size distributions compared to fumed silica. This study also explores a wide range of surface coverages which allows detection of optimum conditions for preparations of the immobilizates. More narrowly focused studies in regard to surface coverage [39, 45, 46] may not allow appreciation of the intricate impact of enzyme properties, surface coverage, and support surface properties on the catalytic competency of the immobilizate. We introduce 3D contour plots to comprehensively correlate visually represent the folding state of inherently different enzyme molecules and the catalytic competency under various regimes of surface coverage. This approach is expected to be extremely useful for emerging applications where subtle changes in the physical or chemical properties of the support need to be evaluated to assure optimal functionality.

Materials and Methods

Materials

Crude CALB (lyophilized; specific activity of 28U/mg solid) and TLL (lyophilized; specific activity of 1400U/mg solid) were obtained from Codexis, Inc. (Pasadena, CA), stored at 4ºC, and used as-received. TLL is a glycosylated monomeric protein with 269 amino acid residues, among them four tryptophans (Trp89, Trp117, Trp221, Trp260) [52-55]. TLL is used for the interesterification and hydrolysis of vegetable oils and animal fats [56]. *Subtilisin Carlsberg* (EC 3.4.21.14; proteinase from *Bacillus licheniformis*; specific activity of 8 U/mg solid), fumed silica (purity of 99.8 wt.%, specific surface area 255 m^2/g, primary particle diameter ~7-50 nm, as reported by the manufacturer), ultrapure Guanidine Hydrochloride (GdmCl), 2,2,2-trifluoroethanol (TFE), and dithiothreitol (DTT) were from Sigma-Aldrich (St. Louis, MO), and used as received. Glass vials (24 mL screw-capped, flat-bottom) were used to prepare the enzyme-fumed silica suspensions.

Unfolding of Enzymes by GdmCl in Aqueous Buffer Solution

The intrinsic fluorescence spectroscopy method to detect unfolding was tested for reference with the powerful denaturant GdmCl in aqueous buffer solution. Unfolding relocates Trp residues [45, 46, 55, 57] which is detectable by fluorescence spectroscopy. Crude enzyme was weighed in a glass vial and 10 mM monobasic phosphate buffer (0.5 to 4.7 mg enzyme/mL, adjusted to pH 7.8 by KOH) containing GdmCl with final concentrations in the range of 1M to 8M was added followed by vortexing for about 30 seconds. Trp is excited at 288 nm. At least five scans were performed and averaged for each sample. Unfolding was monitored in a quartz cuvette (3mm pathlength; Starna Cells, Atascadero CA) by collecting the emission spectrum from 300 to 500 nm (Cary Eclipse spectrofluorimeter, Varian, Cary, NC, 25°C). Excitation and emission bandpasses were set at 5 nm. Maximum emission intensity ($I_{max/em}$) and maximal emission wavelength ($\lambda_{max/em}$) were extracted from the spectra.

Two phenomena have been identified for globular proteins undergoing unfolding initiated by changing from low to high concentrations of GdmCl: 1. Decrease in $I_{max/em}$ and 2. shifting of $\lambda_{max/em}$ towards the red through exposure of the Trp residues to the buffer [54, 55, 58]. **Fig. 1** shows typical tryptophan emission spectra for the unfolding of CALB in aqueous buffer solution by GdmCl from zero to 8M about 30 seconds after the denaturant was added to the enzyme solution. The spectra are assumed to be at equilibrium since no further changes after this measurement were detected over 40 minutes. The decrease in the maximum intensity is attributed to a significant reduction in the quantum yield of the now increasingly exposed Trp residues [54, 55, 58], while the red (right) shifting is attributed to the increased hydrophilicity of the environment surrounding the Trp residues [54, 55, 58]. Inset in **Fig. 1** shows the decrease in $I_{max/em}$ for CALB as the chemically-induced unfolding proceeds. Similar trends were obtained for *s. Carlsberg* and TLL, however, with a less pronounced reduction in intensity most likely due to their rigid structures (data not shown). The enzymes were then ranked in order of increasing conformational stability: CALB, *s. Carlsberg*, TLL. This is corroborated by CALB's plasticity and molecular dynamism [59] as opposed to the rigidity of structurally "hard" *s. Carlsberg* and TLL [31, 60].

Unfolded Fraction Inference for GdmCl Unfolding in Aqueous Buffer Solution

The unfolding data in the presence of GdmCl can be normalized to define an unfolded fraction (ϕ) as follows [45, 46]:

$$\phi_{GdmCl} = 1 - \left(\frac{\mathrm{I^S}_{\lambda} - \mathrm{I^{8M\ GdmCl}}_{\lambda}}{\mathrm{I^N}_{\lambda} - \mathrm{I^{8M\ GdmCl}}_{\lambda}}\right) \qquad \textbf{Equation 1}$$

where $\boldsymbol{\phi_{GdmCl}}$ is the unfolded fraction (0, native; 1, completely unfolded).

$\mathbf{I^S}_{\lambda}$ is the emission intensity at a fixed wavelength for enzyme molecule ensembles at any state of unfolding, $\mathbf{I^N}_{\lambda}$ is the emission intensity at a fixed wavelength for ensembles of native enzyme molecules, and $\mathbf{I^{8M\ GdmCl}}_{\lambda}$ is the emission intensity at a fixed wavelength for fully unfolded enzyme ensembles all in aqueous buffer and in arbitrary units (a.u.).

The wavelength was selected as 330 nm for CALB and TLL and as 305 nm for *s. Carlsberg*. These wavelengths were found to produce the best resolution for detecting different unfolding levels. The ϕ_{GdmCl} values showed a linear dependency on the GdmCl concentration [45, 46] and served as reference to determine the extent of tertiary unfolding in the presence of fumed silica nanoparticles (**Fig. 2**). Similar calibration curves were prepared for other enzyme concentrations as well as for the other enzymes under study.

No significant changes in $\lambda_{max/em}$ were detected for *s. Carlsberg*, which limits the application of this approach for monitoring unfolding under the conditions of our buffer solutions (data not shown).

Baseline for Kinetic Experiments

Buffer only (no enzyme) and nanoparticles in buffer (no enzyme), as well as enzymes in buffer were served as the controls at typical concentrations. These solutions showed no time-dependent change in intensity over 40 minutes as expected [45, 46] leading to the conclusion that all changes with time were attributable to changes in the enzyme molecules introduced by interaction of enzymes, nanoparticles, and added chemicals.

Kinetics of Tertiary Conformational Changes of Enzymes Interacting with Fumed Silica

The time evolution of the tertiary conformational changes of enzymes interacting with fumed silica nanoparticles were monitored by following the emission intensity of Trp residues at a fixed wavelength. Crude enzymes (i.e., CALB, *s. Carlsberg* and TLL) were weighed in a glass vial and 10 mM monobasic phosphate (adjusted to pH 7.8 by KOH) was added followed by vortexing for about 30 seconds. Fumed silica was then added and vortexed until visually homogeneous suspensions were formed (about 30 seconds) as described elsewhere [16-18]. Table 1 shows a summary of the amounts of fumed silica and enzyme used to form the suspensions at the various percentages of nominal surface coverages %SC of enzyme in the final enzyme/fumed silica adsorbates.

The suspensions were transferred to quartz cuvettes and placed in the spectrofluorimeter maintained at 25°C. The excitation was set at 288 nm and the emission recorded at 330 nm for CALB and TLL and at 305 nm for *s. Carlsberg*.

Unfolded Fraction Inference for Kinetic Experiments with Fumed Silica in Aqueous Solution

The kinetics of tertiary deformation of the enzymes in the presence of fumed silica were normalized according to **Equation 2** [45, 46]:

$$\phi_{FS} = 1 - \left(\frac{{\mathrm{I}_{\mathrm{FS}}{}^{\mathrm{S}}}_{\lambda} - {\mathrm{I}^{8\mathrm{M\ GdmCl}}}_{\lambda}}{{\mathrm{I}^{\mathrm{N}}}_{\lambda} - {\mathrm{I}^{8\mathrm{M\ GdmCl}}}_{\lambda}} \right) \qquad \textbf{Equation 2}$$

where $\boldsymbol{\phi_{FS}}$ is the instantaneous unfolded fraction for enzymes in the presence of fumed silica nanoparticles (0, native; 1, completely unfolded).

$\mathbf{I_{FS}}^{\mathbf{S}}{}_{\lambda}$ is the net average emission intensity at a fixed wavelength of enzyme molecule ensembles interacting with fumed silica at any instantaneous state of unfolding (obtained by subtracting the corresponding instantaneous contribution of buffer and nanoparticles), $\mathbf{I}^{\mathbf{N}}{}_{\lambda}$ is the average emission intensity at a fixed wavelength for the ensembles of native enzyme molecules, and $\mathbf{I}^{\mathbf{8M\ GdmCl}}{}_{\lambda}$ is the average emission intensity at a fixed wavelength for fully unfolded enzyme ensembles all in aqueous buffer and in arbitrary units (a.u.).

Regions of Tertiary Conformational Stability: 3D Filled Contour Plots

Enzyme solutions of CALB and *s. Carlsberg* at concentrations of 0.5, 0.7, 3.30, and 4.70 mg/mL were mixed with nanoparticles to form adsorbates with different %SC according to Table 1. For TLL 0.5, 0.7, and 3.30 mg/mL were explored. Each suspension was monitored over about 40 minutes for changes in the tertiary structure via spectrofluorimetry (above). The final equilibrium values for deformation (as a function of total enzyme molecules present) for each enzyme are plotted as the elevation (*z*-direction) of contour plots where the *y*-axis is the concentration of enzyme in the solution at the beginning of preparing the adsorbate and the horizontal *x*-axis represents the expected %SC by the enzyme molecules in the obtained adsorbates (Table 1). **Fig. 3** shows the deformation data for CALB on fumed silica as an example to introduce this type of plot. A total of 20 data points for CALB and *s. Carlsberg*, and 15 points for TLL were used to develop contour plots (see below). An inverse-distance algorithm (SigmaPlot®) was used to interpolate. **Fig. 3** indicates that at low surface coverage deformation becomes very significant, no matter what the initial concentration to prepare the adsorbate was. Detailed discussions follow below.

Results and Discussion

Deformation of Enzymes Interacting with Fumed Silica in Aqueous Solution

Time-dependent fluorescence intensity changes from the Trp residues were used to monitor the structural alteration kinetics of enzymes interacting with fumed silica. Only events after ~30 s could be monitored due to the time needed to mix and vortex suspensions. Baselines for nanoparticle suspensions as well as for the enzyme solutions remained approximately constant as a function of time with a combined error of 7%. Error propagation analysis for the unfolded fraction function (ϕ_{FS}) (**Equation 2**) indicates an error of ~2% or equivalently $\phi_{FS} \pm 0.02$. Deviations from the linear behavior and beyond this error limit can be, therefore, attributed to structural changes.

Fig. 4 compares the time evolution of the unfolding of CALB, *s. Carlsberg* and TLL in the presence of fumed silica. Here, we explore tertiary structural changes of enzymes adsorbing on fumed silica that occur at long time scales (order of several minutes). This time framework encompasses adsorption events that lead to surface saturation as reported previously [16]. In this case, adsorbates forming a low surface coverage of 2%SC are shown. The three enzymes underwent an initial rapid structural change (high initial ϕ_{FS} values). Those initial events are thought to occur within a very short time scale on the order of milliseconds [46] and consequently cannot be tracked with the techniques used in this study.

Unfolding studies by others for proteins adsorbing on colloidal silica nanoparticles revealed rapid initial unfolding for both β lactoglobulin (1200 min) [45] and Cytochrome c (10 min) [39] followed by slower unfolding. For lysozyme (600 min) [46], on the other hand, three events were detected: an initial rapid unfolding followed by a slower refolding, and finally a slow unfolding leading to apparent equilibrium.

Over the initial 20 minutes, CALB molecules undergo both unfolding and refolding until an apparent equilibrium is reached. This might be attributed to the already demonstrated plasticity/dynamism of this enzyme [59]. CALB's structure is composed of seven central β strands flanked by ten α helices [59]. The α5 and α10 are highly mobile regions thought to be involved in CALB's molecular dynamism also demonstrated by CALB's catalytic promiscuity [61]. Trp 113 (detected by our technique) is in close proximity to a mobile α5 region.

An alternative explanation of the unfolding/refolding of CALB is reorientation of CALB molecules on the surface of the nanoparticles towards a low energy state as suggested in the literature ([46] [51]). As opposed to CALB, both TLL and *s. Carlsberg*, showed no significant further conformational changes as indicated by essentially constant ϕ_{FS} values. This is most likely a consequence of the stable structures of these two enzymes. In all cases, no significant net conformational change was observed beyond the initial value.

As shown in **Fig. S1** in Supporting Information, decreasing the amount of nanoparticles to form adsorbates with 100%SC leads to both lower initial and equilibrium deformation was observed for all three enzymes as reported by others [46] for lysozyme adsorbed on colloidal silica nanoparticles at high protein surface concentrations. The lower extent of denaturation was attributed to the higher crowding regime where protein-protein interactions become more dominant and help to stabilize the protein conformation. CALB showed a rapid initial unfolding followed by a slower phase as reported for β lactoglobulin [45]. A significant net unfolding above the initial value was also observed for *s. Carlsberg*. No significant net unfolding for TLL was observed. The equilibrium values of unfolding correlated with the conformational stability or "hardness" of the enzymes. "Hard" TLL unfolded the least while "soft" CALB unfolded the most.

The amount of fumed silica added was decreased even further to form adsorbates with 400%SC (**Fig. S2** in Supporting Information). The equilibrium unfolding values for the three enzymes are quite similar. This further supports the notion that increased protein-protein interaction precludes structural perturbations. The unfolding pathways for CALB and *s. Carlsberg* show logarithmic trends over time. This can be attributed to a two-stage model of unfolding [39]. The unfolding trace for TLL is essentially horizontal and consequently reflects no significant net unfolding with respect to the initial value.

Regions of Tertiary Conformational Stability for Enzyme/Fumed Silica Adsorbates

A general view of tertiary conformational stability for the three hydrolases adsorbing on fumed silica was obtained by conducting multiple unfolding experiments for various surface coverages and enzyme concentrations according to Table 1. **Fig. 5** combines the equilibrium values of unfolding for CALB. Two different regions of conformational stability are observed at surface coverage values above and below approximately 200%SC (vertical dotted line). Adsorbates obtained at high surface coverages (i.e., above 200%SC) exhibit highly stable conformations (region III). The tertiary structure remains essentially intact in this region (lighter shading). Below 200%SC (region I), however, the adsorbed enzymes deform significantly (darker areas). Some may even appear to be completely denatured at very low surface coverages as indicated by ϕ_{FS} values near unity. Region II is a transitional region. Adsorbates with different %SC have been previously obtained along the diagonal line (**Fig. 5**). The catalytic competency of these lyophilized adsorbates in hexane [16] is schematically shown in the inset (**Fig. 5**). The three regimes of surface loading and the catalytic competency can be linked: 1. (enzyme conformation controlled, region I) low surface coverages where the enzyme molecules have enough space to maximize their contact with the surface. This can alter the native conformation especially for "soft" enzymes thereby leading to reduced catalytic activity while "hard" enzymes suffer less impact [17], 2. intermediate surface coverages (region II) have active enzyme conformations where enzyme-enzyme interactions stabilize even "soft" enzymes and prevent excessive surface interactions, and 3. (reactions are diffusion controlled, region III) high surface coverages where the enzyme molecules are densely packed in multi-layers on the surface leading to mass transfer limitation of catalysis. [62].

The usefulness of the above introduced 3D contour diagrams to correlate conformational stability and catalytic competency was further exploited with "hard" *s. Carlsberg* and TLL. As shown in **Fig. S3** in Supporting Information, *s. Carlsberg* also shows three regions of conformational stability but *s. Carlsberg* shows more resilience against denaturation in region I where the "soft" CALB denatures strongly. Catalytic competency of lyophilized preparations of *s. Carlsberg* along the diagonal in **Fig. S3** is shown in the inset (**Fig. S3**), corroborating that *s. Carlsberg* shows high catalytic competency at low surface coverage which would denature CALB. A similar diagram for TLL is shown in **Fig. S4** in Supporting Information. TLL exhibits three regions of conformational stability similar to the enzymes discussed above. Region I, however, has only partially altered enzyme conformations as evident from a maximum $\boldsymbol{\phi_{FS}}$ value of 0.6. This is perhaps not surprising for the enzyme with the least tendency to denature of the three considered here. This finding also further supports the proposed relationship between the inherent conformational stability of enzyme molecules and their tendency to undergo conformational changes upon contact with solid surfaces. While "soft" enzymes require intermediate surface coverage to stabilize them, “hard” enzymes exhibit well maintained structures already at low surface coverage.

In summary, our findings confirm the critical role that the surface area availability plays by defining the physical arrangement of the enzyme molecules on the surface of the nanoparticles. Additionally, visualizing conformational stability regions as a function of the surface packing density and further correlation with activity data can be facilitated with the aid of the 3D contour diagrams introduced here.

Impact of Tertiary Structure Modifiers for Enzymes Interacting with Fumed Silica in Aqueous Solution

Tertiary structure modifiers (2,2,2-trifluoroethanol (TFE) and Dithiothreitol (DTT)) can be added prior to adsorption on fumed silica to gain more insight into the type of intermolecular interactions predominating during the adsorption process. TFE induces structural changes in hydrophobic protein segments while DTT reduces disulfide bonds to the unbounded thiols. The time dependent conformational changes of the three enzymes in the presence of 30% (v/v) TFE for adsorbates with a 100%SC is shown in **Fig. 6** panel A. Addition of TFE to both *s. Carlsberg* and TLL resulted in increased initial values of deformation (data in the absence of TFE is superimposed in **Fig. 6** panel A). The shape of the absorbance changes for these two enzymes were similar to those in the absence of TFE, i.e., logarithmic for *s. Carlsberg* and linear for TLL. Overall, the extent of denaturation substantially increased over the initial values (40% and 30% for *s. Carlsberg* and TLL, respectively). This most likely indicates that the disrupting intramolecular contacts hasten denaturation, suggesting that these contact regions are responsible for stabilizing the structures of these two enzymes.

The initial impact of TFE on CALB unfolding was essentially negligible and some refolding is observed, likely due to the different content of groups in CALB that interact strongly with TFE.

The presence of DTT showed no significant impact on the time-course and extent of unfolding for *s. Carlsberg* and TLL (**Fig. 6** panel B). This is most likely due to the absence of thiol sensitive disulfide bonds. CALB, on the other hand, contains DTT-sensitive disulfide bridges and showed decreased initial and equilibrium unfolding values (**Fig. 6** panel B). The exposed residues are then available for interaction with the nanoparticles. This further supports the notion that increased interactions lead to repression of dynamism and ultimately to less opportunities for continued unfolding. This could also explain why the observed DTT-disrupted CALB unfolding pathway resembles those of the "hard" enzymes. The exposure of regions suitable for interaction with the surface is therefore likely to occur more gradually in the presence of DTT.

Regions of Conformational Stability for Enzyme/Fumed Silica Adsorbates in the Presence of Structure Modifiers

Fig. 7 panel A shows that the region III originally observed for CALB was destabilized by TFE. It is likely that groups exposed by TFE facilitated additional opportunities for unfolding by increasing the affinity towards the hydrophilic solid surface. The unfolding extent in this region increased by nearly 50% with respect to the absence of TFE (**Fig. 5**).

Fig. 7 panel B summarizes the impact of DTT on CALB's tertiary structure. Once disulfide bridges are disrupted, CALB's structure is destabilized and some previously occluded regions are exposed. The extent of unfolding in the lower part of regions II and III (i.e., below 2.5 mg/mL and surface coverages above 100%SC) remains low. This could support the argument that the DTT-induced destabilization of CALB may possibly be compensated by interactions with the neighboring molecules. This further supports the idea that protein-protein interactions outweigh protein-surface interactions in region III.

As the enzyme concentration increases, the extent of unfolding also increases at both low and high surface coverages (upper part of regions I and III in **Fig. 7** panel B). The accessibility of DTT to the enzyme at high enzyme concentrations is likely to be compromised by the crowding of enzyme molecules. This leads to a behavior resembling that of the enzyme molecules in the absence of DTT.

A similar study with structural modifiers was conducted for *s. Carlsberg*. As in the case of CALB, the exposure of hydrophobic groups leads to a substantial loss of conformational stability at high surface coverages (data not shown). Due to the tightly packed structure of *s. Carlsberg*, the exposure of hydrophobic groups is rapid. This led to a relatively higher net unfolding than that observed for CALB in this region. Below 100%SC, unfolding was reduced when compared with the enzyme in the absence of TFE. This could be also a direct consequence of the rapid initial unfolding. Once fully extended binding is promoted at the outset of the experiment, the unfolded enzyme molecule's structure is rapidly attached to the abundant solid surface area provided in this region. No additional opportunities are present that would allow for further unfolding. The case of DTT-induced conformational changes for *s. Carlsberg* is very different. Due to the lack of open moieties on the structure suitable for reduction, no major changes were observed and the regions of stability remained essentially unaffected (data not shown).

Conclusions

We have shown evidence that the extent of tertiary conformational changes of three hydrolases adsorbed on fumed silica is mainly dependent on the density of the surface covered by the enzyme molecules, which is described here as a nominal surface coverage (%SC), and the inherent conformational stability and dynamics of the enzyme molecules ("hardness"). At low %SC, the unfolding pathway of CALB, a "soft" enzyme, on fumed silica showed continuous unfolding/refolding events. This was attributed to CALB's conformationally dynamic and fluctuating structure. "Hard" *s. Carlsberg* and TLL, in contrast, exhibited approximately linear unfolding with time which was attributed to their higher inherent conformational stabilities. When moving to high %SC, the unfolding pathways exhibited fewer fluctuations due to stabilizing protein-protein interactions.

Three regions of conformational stability were identified for the three hydrolases at equilibrium with the aid of 3D conformational diagrams: I. a region at low % SC where adsorbates of "soft" CALB exhibited low conformational stability most likely due to multi-point attachment to the surface, II. a region of transitional stability at an intermediate %SC (~200%SC), and III. a region of high stability at high %SC where protein-protein interactions exert a stabilizing effect. These regions correlated well the observed apparent catalytic activity in hexane. The low stability region correlated well with poorly active preparations due to denaturation for "soft" CALB, the transitional region with an optimal in activity, and the high stability region with low CALB catalytic activity due to mass-transfer limitations. In the case of "hard" *s. Carlsberg*, resilience to denaturation at low %SC when compared to CALB explained the constantly increasing apparent catalytic activity observed in this surface loading regime.

Details of the structural interactions were further resolved by adding TFE and DTT to the adsorbing mixtures. TFE exposed hydrophobic segments that for all enzymes appeared to help to stabilize the structure in the “crowded surface” Region III. In the sparsely populated surface Region I, the maximum extent of unfolding for both CALB and *s. Carlsberg* was reduced. This was explained by lower content of interacting groups for CALB and by a rapid attachment of the rigid unfolded state for *s. Carlsberg*. The addition of DTT to CALB’s adsorbing mixtures showed no significant impact in the unfolding levels in the lower part of region III, which confirmed that protein-protein interactions outweigh surface-protein interactions in this region. Upon DTT-induced disruption, Region I showed less unfolding most likely due to a gradual attachment of the very flexible unfolded state of CALB. This was corroborated with unfolding pathways that resemble those of “hard” enzymes.

The complex enzyme/solid interactions in regard to catalytic activity that were investigated here can be used to rationalize and optimize catalysis with enzymes in solvents. The conclusion that for “soft” enzymes there is an optimum enzyme/surface area ratio for immobilization while there is not for “hard” enzymes appears not obvious.

References

[1] M.N. Gupta, Enzyme Function in Organic-Solvents, Eur. J. Biochem., 203 (1992) 25-32.

[2] A. Zaks and A.J. Russell, Enzymes in Organic-Solvents - Properties and Applications, J. Biotechnol., 8 (1988) 259-270.

[3] H. Kise, Ester and Peptide-Synthesis by Proteases in Organic-Solvents, Journal of Synthetic Organic Chemistry Japan, 49 (1991) 42-51.

[4] R. Fernandezlafuente, C.M. Rosell and J.M. Guisan, Enzyme Reaction-Engineering - Synthesis of Antibiotics Catalyzed by Stabilized Penicillin-G Acylase in the Presence of Organic Cosolvents, Enzyme Microb. Technol., 13 (1991) 898-905.

[5] Y.L. Khmelnitsky and J.O. Rich, Biocatalysis in nonaqueous solvents, Curr. Opin. Chem. Biol., 3 (1999) 47-53.

[6] J.O. Rich and Y.L. Khmelnitsky, Phospholipase D-catalyzed transphosphatidylation in anhydrous organic solvents, Biotechnol. Bioeng., 72 (2001) 374-377.

[7] A.M. Klibanov, Asymmetric enzymatic oxidoreductions in organic solvents, Curr. Opin. Biotechnol., 14 (2003) 427-431.

[8] M.S. Antczak, A. Kubiak, T. Antczak and S. Bielecki, Enzymatic biodiesel synthesis - Key factors affecting efficiency of the process, Renew. Energy, 34 (2009) 1185-1194.

[9] J.E. Puskas, M.Y. Sen and K.S. Seo, Green Polymer Chemistry Using Nature's Catalysts, Enzymes, J. Polym. Sci. Pol. Chem., 47 (2009) 2959-2976.

[10] A.M. Klibanov, Improving enzymes by using them in organic solvents, Nature, 409 (2001) 241-246.

[11] A.M. Klibanov, Why are enzymes less active in organic solvents than in water?, Trends Biotechnol., 15 (1997) 97-101.

[12] J.A. Bosley and A.D. Peilow, Immobilization of lipases on porous polypropylene: Reduction in esterification efficiency at low loading, J. Am. Oil Chem. Soc., 74 (1997) 107-111.

[13] B. Chen, J. Hu, E.M. Miller, W.C. Xie, M.M. Cai and R.A. Gross, Candida antarctica lipase B chemically immobilized on epoxy-activated micro- and nanobeads: Catalysts for polyester synthesis, Biomacromolecules, 9 (2008) 463-471.

[14] B. Chen, E.M. Miller, L. Miller, J.J. Maikner and R.A. Gross, Effects of macroporous resin size on Candida antarctica lipase B adsorption, fraction of active molecules, and catalytic activity for polyester synthesis, Langmuir, 23 (2007) 1381-1387.

[15] B. Chen, M.E. Miller and R.A. Gross, Effects of porous polystyrene resin parameters on Candida antarctica Lipase B adsorption, distribution, and polyester synthesis activity, Langmuir, 23 (2007) 6467-6474.

[16] J.C. Cruz, P.H. Pfromm and M.E. Rezac, Immobilization of Candida antarctica Lipase B on fumed silica, Process Biochem., 44 (2009) 62-69.

[17] K. Wurges, P.H. Pfromm, M.E. Rezac and P. Czermak, Activation of subtilisin Carlsberg in hexane by lyophilization in the presence of fumed silica, J. Mol. Catal. B: Enzym., 34 (2005) 18-24.

[18] P.H. Pfromm, M.E. Rezac, K. Wurges and P. Czermak, Fumed silica activated subtilisin Carlsberg in hexane in a packed-bed reactor, Aiche J., 53 (2007) 237-242.

[19] P. Wang, Nanoscale biocatalyst systems, Curr. Opin. Biotechnol., 17 (2006) 574-579.

[20] R.K. Iler, The Chemistry of Silica, John Wiley & Sons, Inc., 1979.

[21] V.M. Gun'ko, I.F. Mironyuk, V.I. Zarko, V.V. Turov, E.F. Voronin, E.M. Pakhlov, E.V. Goncharuk, R. Leboda, J. Skubiszewska-Zieba, W. Janusz, S. Chibowski, Y.N. Levchuk and

A.V. Klyueva, Fumed silicas possessing different morphology and hydrophilicity, J. Colloid Interface Sci., 242 (2001) 90-103.

[22] V.M. Gun'ko, I.F. Mironyuk, V.I. Zarko, E.F. Voronin, V.V. Turov, E.M. Pakhlov, E.V. Goncharuk, Y.M. Nychiporuk, N.N. Vlasova, P.P. Gorbik, O.A. Mishchuk, O.A. Mishchuk, A.A. Chuiko, T.V. Kulik, B.B. Palyanytsya, S.V. Pakhovchishin, J. Skubiszewska-Zieba, W. Janusz, A.V. Turov and R. Leboda, Morphology and surface properties of fumed silicas, J. Colloid Interface Sci., 289 (2005) 427-445.

[23] V.M. Gun'ko, E.F. Voronin, L.V. Nosach, E.M. Pakhlov, N.V. Guzenko, R. Leboda and J. Skubiszewska-Zieba, Adsorption and migration of poly(vinyl pyrrolidone) at a fumed silica surface, Adsorpt. Sci. Technol., 24 (2006) 143-157.

[24] V.M. Gun'ko, V.I. Zarko, E.F. Voronin, E.V. Goncharuk, L.S. Andriyko, N.V. Guzenko, L.V. Nosach and W. Janusz, Successive interaction of pairs of soluble organics with nanosilica in aqueous media, J. Colloid Interface Sci., 300 (2006) 20-32.

[25] V.M. Gun'ko, V.I. Zarko, E.F. Voronin, V.V. Turov, I.F. Mironyuk, Gerashchenko, II, E.V. Goncharuk, E.M. Pakhlov, N.V. Guzenko, R. Leboda, J. Skubiszewska-Zieba, W. Janusz, S. Chibowski, Y.N. Levchuk and A.V. Klyueva, Impact of some organics on structural and adsorptive characteristics of fumed silica in different media, Langmuir, 18 (2002) 581-596.

[26] M.T. Ru, S.Y. Hirokane, A.S. Lo, J.S. Dordick, J.A. Reimer and D.S. Clark, On the salt-induced activation of lyophilized enzymes in organic solvents: Effect of salt kosmotropicity on enzyme activity, J. Am. Chem. Soc., 122 (2000) 1565-1571.

[27] M.T. Ru, K.C. Wu, J.P. Lindsay, J.S. Dordick, J.A. Reimer and D.S. Clark, Towards more active biocatalysts in organic media: Increasing the activity of salt-activated enzymes, Biotechnol. Bioeng., 75 (2001) 187-196.

[28] J. Uppenberg, M.T. Hansen, S. Patkar and T.A. Jones, Sequence, Crystal-Structure Determination and Refinement of 2 Crystal Forms of Lipase-B From *Candida antarctica*, Structure, 2 (1994) 293-308.

[29] D.J. Neidhart and G.A. Petsko, The Refined Crystal-Structure of Subtilisin Carlsberg at 2.5 A Resolution, Protein Eng., 2 (1988) 271-276.

[30] J.K.A. Kamal, T.B. Xia, S.K. Pal, L. Zhao and A.H. Zewail, Enzyme functionality and solvation of Subtilisin Carlsberg: from hours to femtoseconds, Chem. Phys. Lett., 387 (2004) 209-215.

[31] A.K. Shaw and S.K. Pal, Activity of Subtilisin Carlsberg in macromolecular crowding, J. Photochem. Photobiol., B, 86 (2007) 199-206.

[32] P. Asuri, S.S. Bale, S.S. Karajanagi and R.S. Kane, The protein-nanomaterial interface, Curr. Opin. Biotechnol., 17 (2006) 562-568.

[33] P. Asuri, S.S. Bale, R.C. Pangule, D.A. Shah, R.S. Kane and J.S. Dordick, Structure, function, and stability of enzymes covalently attached to single-walled carbon nanotubes, Langmuir, 23 (2007) 12318-12321.

[34] P. Asuri, S.S. Karajanagi, A.A. Vertegel, J.S. Dordick and R.S. Kane, Enhanced stability of enzymes adsorbed onto nanoparticles, J. Nanosci. Nanotechnol., 7 (2007) 1675-1678.

[35] P. Singh, A. Rao, V. Dutta, M. Gupta and S. Raghava, Nanoparticles of unmodified titanium dioxide facilitate protein refolding, J. Mater. Chem., 19 (2009) 2830-2834.

[36] R.S. Kane and A.D. Stroock, Nanobiotechnology: Protein-nanomaterial interactions, Biotechnol. Prog., 23 (2007) 316-319.

[37] W. Norde and J.P. Favier, Structure of Adsorbed and Desorbed Proteins, Colloids Surf., B 64 (1992) 87-93.

[38] W. Shang, J.H. Nuffer, J.S. Dordick and R.W. Siegel, Unfolding of ribonuclease A on silica nanoparticle surfaces, Nano Lett., 7 (2007) 1991-1995.

[39] W. Shang, J.H. Nuffer, V.A. Muniz-Papandrea, W. Colon, R.W. Siegel and J.S. Dordick, Cytochrome c on Silica Nanoparticles: Influence of Nanoparticle Size on Protein Structure, Stability, and Activity, Small, 5 (2009) 470-476.

[40] J.L. West and N.J. Halas, Engineered nanomaterials for biophotonics applications: Improving sensing, imaging, and therapeutics, Annu. Rev. Biomed. Eng., 5 (2003) 285-292.

[41] H.J. Lewerenz, Enzyme-semiconductor interactions: Routes from fundamental aspects to photoactive devices, Phys. Status Solidi B-Basic Solid State Phys., 245 (2008) 1884-1898.

[42] H.L. Su, R. Yuan, Y.Q. Chai, Y. Zhuo, C.L. Hong, Z.Y. Liu and X. Yang, Multilayer structured amperometric immunosensor built by self-assembly of a redox multi-wall carbon nanotube composite, Electrochim. Acta, 54 (2009) 4149-4154.

[43] N. Chopra, V.G. Gavalas, B.J. Hinds and L.G. Bachas, Functional one-dimensional nanomaterials: Applications in nanoscale biosensors, Anal. Lett., 40 (2007) 2067-2096.

[44] A. Ganesan, B.D. Moore, S.M. Kelly, N.C. Price, O.J. Rolinski, D.J.S. Birch, I.R. Dunkin and P.J. Halling, Optical Spectroscopic Methods for Probing the Conformational Stability of Immobilised Enzymes, Chemphyschem, 10 (2009) 1492-1499.

[45] X. Wu and G. Narsimhan, Characterization of secondary and tertiary conformational changes of beta-lactoglobulin adsorbed on silica nanoparticle surfaces, Langmuir, 24 (2008) 4989-4998.

[46] X.Y. Wu and G. Narsimhan, Effect of surface concentration on secondary and tertiary conformational changes of lysozyme adsorbed on silica nanoparticles, Biochim. Biophys. Acta, Proteins Proteomics, 1784 (2008) 1694-1701.

[47] A. Ganesan, N.C. Price, S.M. Kelly, I. Petry, B.D. Moore and P.J. Halling, Circular dichroism studies of subtilisin Carlsberg immobilised on micron sized silica particles, Biochim. Biophys. Acta, Proteins Proteomics, 1764 (2006) 1119-1125.

[48] K. Hidajat, M. Uddin and Z. Peng, Conformational change of adsorbed and desorbed bovine serum albumin on nano-sized magnetic particles, Colloids Surf., B, 33 (2004) 15-21.

[49] N. Shamim, H. Liang, K. Hidajat and M.S. Uddin, Adsorption, desorption, and conformational changes of lysozyme from thermosensitive nanomagnetic particles, J. Colloid Interface Sci., 320 (2008) 15-21.

[50] A. Kondo, S. Oku and K. Higashitani, Structural-Changes in Protein Molecules Adsorbed on Ultrafine Silica Particles, J. Colloid Interface Sci., 143 (1991) 214-221.

[51] N. Tokuriki and D.S. Tawfik, Protein Dynamism and Evolvability, Science, 324 (2009) 203-207.

[52] P. Hoyrup, S. Patkar, J. Vind, A. Svendsen, K. Hult and E. Hedin, Implications of surface charge and curvature for the binding orientation of Thermomyces lanuginosus lipase on negatively charged or zwitterionic phospholipid vesicles as studied by ESR spectroscopy, Biochemistry, 44 (2005) 16658-16671.

[53] A. Jutila, K. Zhu, S.A. Patkar, J. Vind, A. Svendsen and P.K.J. Kinnunen, Detergent-induced conformational changes of Humicola lanuginosa lipase studied by fluorescence spectroscopy, Biophys. J., 78 (2000) 1634-1642.

[54] A. Jutila, K. Zhu, E.K.J. Tuominen and P.K.J. Kinnunen, Fluorescence spectroscopic characterization of Humicola lanuginosa lipase dissolved in its substrate, Biochim. Biophys. Acta, Proteins Proteomics, 1702 (2004) 181-189.

[55] K. Zhu, A. Jutila and P.K.J. Kinnunen, Steady state and time resolved effects of guanidine hydrochloride on the structure of Humicola lanuginosa lipase revealed by fluorescence spectroscopy, Protein Sci., 9 (2000) 598-609.

[56] T. Schafer, T.W. Borchert, V.S. Nielsen, P. Skagerlind, K. Gibson, K. Wenger, F. Hatzack, L.D. Nilsson, S. Salmons, S. Pedersen, H.P. Heldt-Hansen, P.B. Poulsen, H. Lund, K.M. Oxenboll, G.F. Wu, H.H. Pedersen and H. Xu, Industrial enzymes, in: White Biotechnology, Vol 105, Springer-Verlag Berlin, Berlin, 2007, pp. 59-131.

[57] P. Acharya and N.M. Rao, Stability studies on a lipase from Bacillus subtilis in guanidinium chloride, J. Protein Chem., 22 (2003) 51-60.

[58] T. De Diego, P. Lozano, S. Gmouh, M. Vaultier and J.L. Iborra, Understanding structure - Stability relationships of Candida antartica lipase B in ionic liquids, Biomacromolecules, 6 (2005) 1457-1464.

[59] M. Skjot, L. De Maria, R. Chatterjee, A. Svendsen, S.A. Patkar, P.R. Ostergaard and J. Brask, Understanding the Plasticity of the alpha/beta Hydrolase Fold: Lid Swapping on the Candida antarctica Lipase B Results in Chimeras with Interesting Biocatalytic Properties, ChemBioChem, 10 (2009) 520-527.

[60] A.W. Sonesson, T.H. Callisen, H. Brismar and U.M. Elofsson, Lipase surface diffusion studied by fluorescence recovery after photobleaching, Langmuir, 21 (2005) 11949-11956.

[61] C. Carboni-Oerlemans, P.D. de Maria, B. Tuin, G. Bargeman, A. van der Meer and R. van Gemert, Hydrolase-catalysed synthesis of peroxycarboxylic acids: Biocatalytic promiscuity for practical applications, J. Biotechnol., 126 (2006) 140-151.

[62] L. Cao, Adsorption-based Immobilization, in: Carrier-bound Immobilized Enzymes: Principles, Applications and Design, Vol 1, Wiley-VCH Verlag GmbH & Co. KGaA, Germany, Weinheim, 2005, pp. 53-168.

[63] U. Derewenda, L. Swenson, R. Green, Y. Wei, S. Yamaguchi, R. Joerger, M.J. Haas and Z.S. Derewenda, Current Progress in Crystallographic Studies of New Lipases from Filamentous Fungi, Protein Eng., 7 (1994) 551-557.

Tables

Table 1

Summary of the amounts of fumed silica and enzyme employed to form the suspensions with different nominal surface coverages. The enzyme concentration for each suspension was varied from 0.5 mg/mL to 4.70 mg/mL.

		Mass fumed silica (g)					
Enzyme	**Enzyme mass (mg)**	2%SC*	17%SC	100%SC	230%SC	400%SC	1250%SC
CALB	7	0.718	0.092	0.016	0.0068	0.0039	0.0013
TLL	5	0.350	0.040	0.010	0.0030	0.0018	0.0006
s. Carlsberg	5	0.315	0.036	0.009	0.0027	0.0016	0.0005

* The Nominal Surface Coverage (% SC) was calculated as follows:

$$\%SC = \frac{Projected\ area\ of\ enzyme\ molecule}{Nominal\ surface\ area\ of\ Fumed\ Silica} * 100 \qquad \text{Equation 3}$$

The projected area of enzyme is calculated assuming a spherical shape for the enzyme molecules. The diameter of the enzyme molecules from crystallographic data were 6.4 nm [28], 5.0 nm [63], and 4.2 nm [29] for CALB, TLL and *s. Carlsberg*, respectively. The nominal surface area of fumed silica is as provided by the manufacturer: 255m^2/g.

Figure Captions

Fig. 1. Tryptophan fluorescence spectrum of the unfolding of CALB induced by GdmCl in aqueous buffer solution. (○) Native, (□) 1M GdmCl, (Δ) 2M GdmCl, (×) 4M GdmCl and (∗) 8M GdmCl. Decrease in the maximum emission intensity ($I_{max/em}$) of Trp residues due to GdmCl-induced denaturation is shown in the inset. *y*-error bars represent the standard error of multiple analyses of identical samples. Enzyme concentration was maintained at 0.5 mg/ml and pH 7.8.

Fig. 2. Normalized fluorescence intensity for the GdmCl induced unfolding of CALB in aqueous buffer. The tryptophan emission was monitored at 330 nm. Measurements were carried out at enzyme concentration of 0.5 mg/mL and pH 7.8. Similar calibration curves were obtained for *s. Carlsberg* and TLL (data not shown).

Fig. 3. Unfolding data for CALB on fumed silica (*z*-axis) as a function of initial enzyme concentration (*y*-axis) and nominal surface coverage (*x*-axis). These data will be shown in 3D contour plots to identify regions of conformational stability and to subsequently correlate them with the surface loading regimes previously postulated for the lyophilized adsorbates.

Fig. 4. Unfolding kinetics of (●) CALB, (□) *s. Carlsberg* and (Δ) TLL adsorbing on fumed silica nanoparticles to form adsorbates with a nominal surface coverage of 2%SC. Data is normalized with the corresponding calibration curves and subsequently expressed as unfolded fraction. Enzyme concentration was maintained at 0.5 mg/mL and pH at 7.8.

Fig. 5. Regions of conformational stability for CALB/Fumed Silica adsorbates. The dotted vertical line at ~200%SC separates two different regions of conformational stability: **Region I** delimited by a long-dash-dot line where adsorbates exhibit low conformational stability, and **Region III** delimited by a short-dash-dot line where adsorbates have highly stable conformations. The presence of these two regions is likely to be responsible for the observed catalytic activity ($\mathbf{r_0}$) of the lyophilized adsorbates in hexane (inset). The low catalytic activity observed at low %SC can be linked to **Region I**. Even though the structure is well preserved in **Region III**, multi-layer packing is likely responsible for diffusional limitations of catalysis. The maximum in activity between those two regions can be attributed to an optimal arrangement on the surface where the structure is relatively well maintained without excessive clustering (**Region II**, delimited by a dotted line).

Fig. 6. Unfolding kinetics of hydrolases adsorbing on fumed silica nanoparticles in the presence of tertiary structure modifiers: (A) 30% (v/v) TFE and (B) 0.5 mg/mL DTT: (O) CALB, (■) *s. Carlsberg* and (▲) TLL. Data for unfolding in the absence of modifiers is superimposed for comparison: (●) CALB, (□) *s. Carlsberg* and (Δ) TLL. Components were mixed to form a nominal surface coverage of 100%SC. Data is normalized with the corresponding calibration curves and subsequently expressed as unfolded fraction. Enzyme concentration was maintained at 0.7 mg/mL and pH at 7.8.

Fig. 7. Impact of tertiary structure modifiers on conformational regions of CALB/FS adsorbates. This was tested by forming buffered suspensions with (A) 30%(v/v) TFE and (B) 0.5 mg/mL DTT. The previously identified **Region III** exhibits a higher unfolding in the presence of TFE. The extent of unfolding in **Region I** decreased in the presence of TFE. The addition of DTT

resulted in a substantially large **Region III** for low %SC and low concentrations. The same type of lines as those in **Fig. 5** were used to delimit the regions of conformational stability.

Supporting Information

Conformational Changes and Catalytic Competency of Hydrolases Adsorbing on Fumed Silica Nanoparticles: I. Tertiary Structure

Juan C. Cruz[1], Peter H. Pfromm[1]*, John M. Tomich[2], Mary E. Rezac[1]

(1) Department of Chemical Engineering, Kansas State University, 1005 Durland Hall, Manhattan, KS 66506 - 5106, USA.

(2) Department of Biochemistry and Biotechnology/Proteomics Core Facility, Kansas State University, Burt Hall, KS 66506 - 5106, USA.

Fig. S1. Unfolding kinetics of ♦) CALB, (□) *s. Carlsberg* and (Δ) TLL adsorbing of fumed silica nanoparticles to form adsorbates with a nominal surface coverage of 100%SC. Data is normalized with the corresponding calibration curves and subsequently expressed as unfolded fraction using Equation 2. Enzyme concentration was maintained at 0.5 mg/mL and pH at 7.8.

Fig. S2. Unfolding kinetics of (●) CALB, (□) s. Carlsberg and (Δ) TLL adsorbed of fumed silica nanoparticles to obtain a nominal surface coverage of 400%SC. Data is normalized with the corresponding calibration curves and subsequently expressed as unfolded fraction using Equation 2. Enzyme concentration was maintained at 0.5 mg/mL and pH at 7.8.

Fig. S3. Regions of conformational stability for *s. Carlsberg*/Fumed Silica adsorbates. The dotted vertical line at ~200%SC separates two different regions of conformational stability: **Region I and III** of low and high conformational stability, respectively. In this case, the catalytic activity ($\mathbf{r_0}$) of the lyophilized adsorbates in hexane (inset) is constantly increasing. As opposed to CALB, only partially unfolded enzyme molecules are present in the lower part of **Region I** at low initial enzyme concentrations. This resilience to denaturation could explain the higher activities observed for lyophilized adsorbates of *s. Carlsberg* at low surface coverages. The same type of lines as those in **Fig. 5** were used to delimit the regions of conformational stability.

Fig. S4. Regions of conformational stability for TLL/Fumed Silica adsorbates. The dotted vertical line at ~250%SC separates two different regimes of conformational stability: **Region I and III** of low and high conformational stability, respectively. Across the whole **Region I** only partially unfolded conformations (ϕ_{FS} ~0.6) were identified, which confirms the resilience of highly stable enzymes to denature at low surface coverages. The same type of lines as those in **Fig. 5** were used to delimit the regions of conformational stability.

Fig. 1

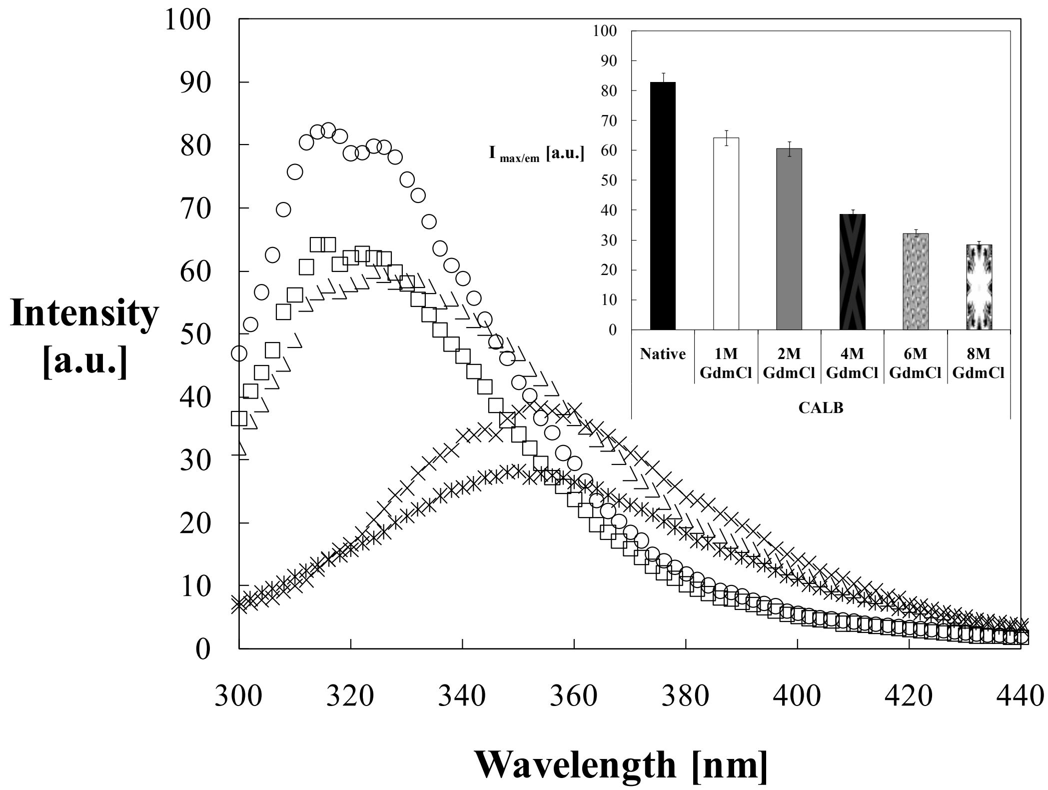
Intensity [a.u.]
Wavelength [nm]
I max/em [a.u.]
Native
1M GdmCl
2M GdmCl
4M GdmCl
6M GdmCl
8M GdmCl
CALB

Fig. 2

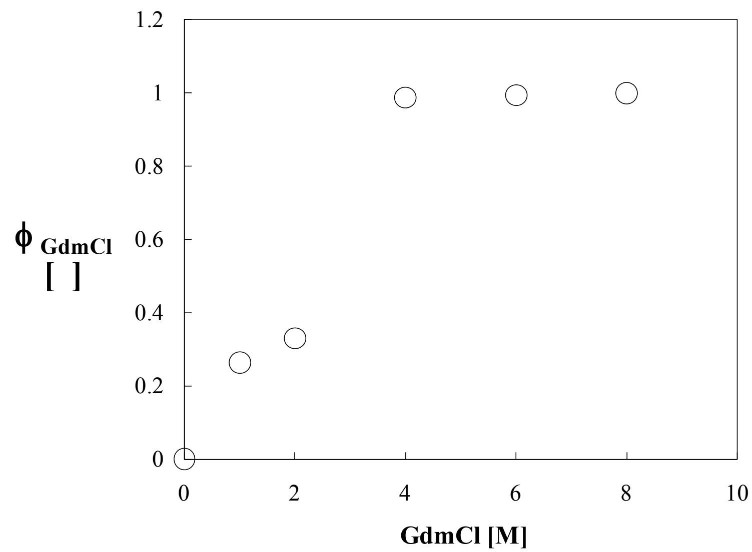

Fig. 3

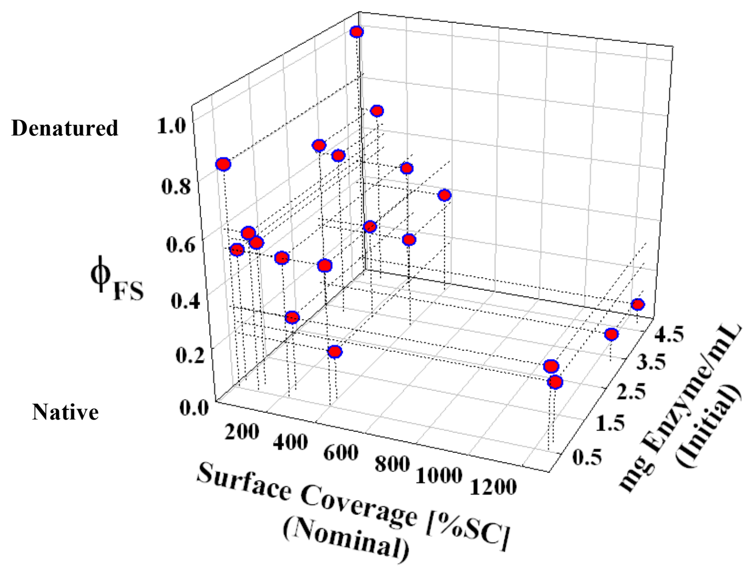
Denatured
Native
1.0
0.8
0.6
0.4
0.2
0.0
ϕ_{FS}
200
400
600
800
1000
1200
Surface Coverage [%SC]
(Nominal)
0.5
1.5
2.5
3.5
4.5
mg Enzyme/mL
(Initial)

Fig. 4

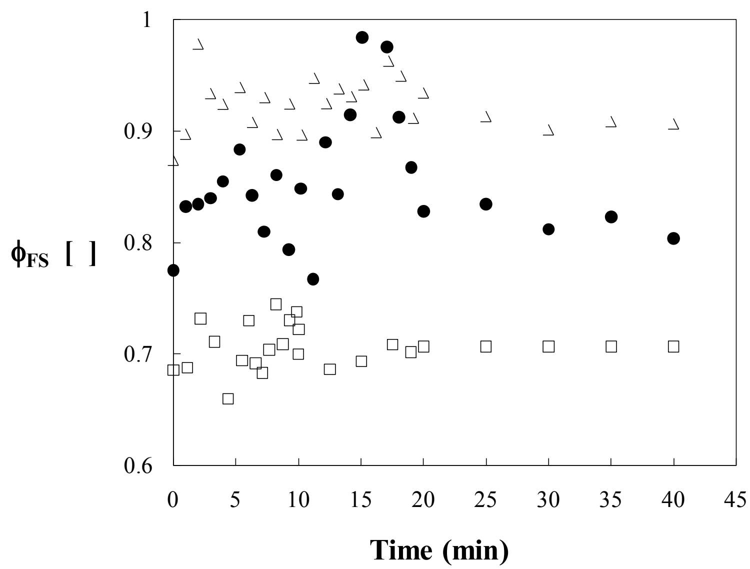

Fig. 5

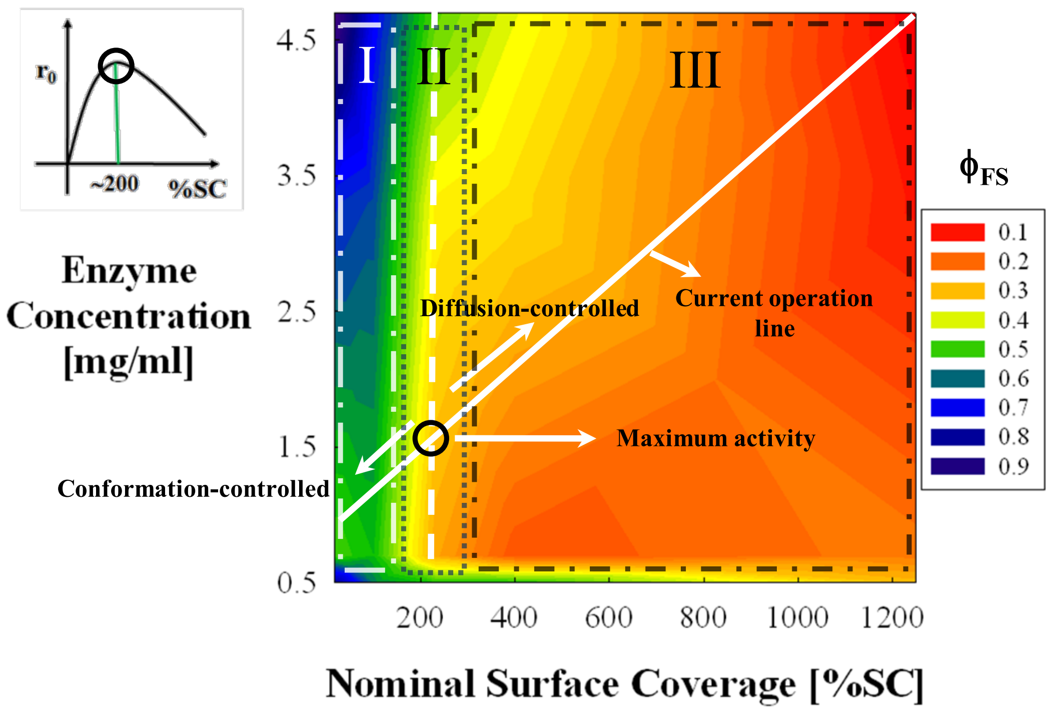

r0
~200
%SC
Enzyme Concentration [mg/ml]
4.5
3.5
2.5
1.5
0.5
I
II
III
Diffusion-controlled
Current operation line
Maximum activity
Conformation-controlled
200
400
600
800
1000
1200
Nominal Surface Coverage [%SC]
ϕFS
0.1
0.2
0.3
0.4
0.5
0.6
0.7
0.8
0.9

Fig. 6

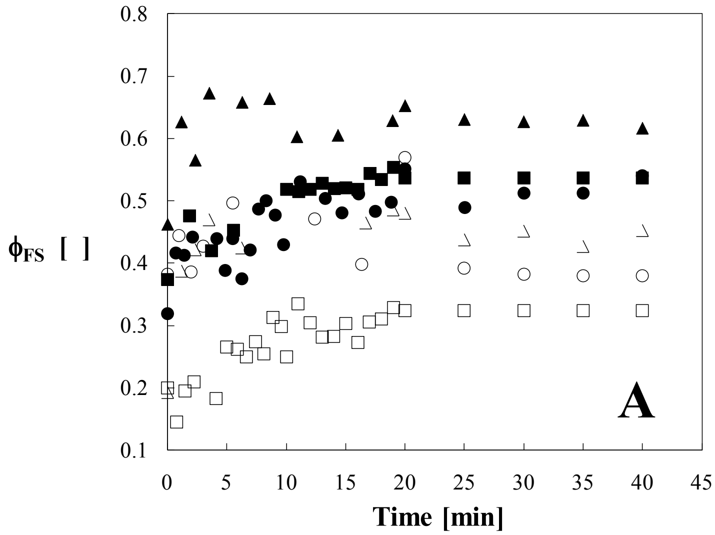

0.8
0.7
0.6
0.5
0.4
0.3
0.2
0.1
ϕ_{FS} [ ]
0
5
10
15
20
25
30
35
40
45
Time [min]
A

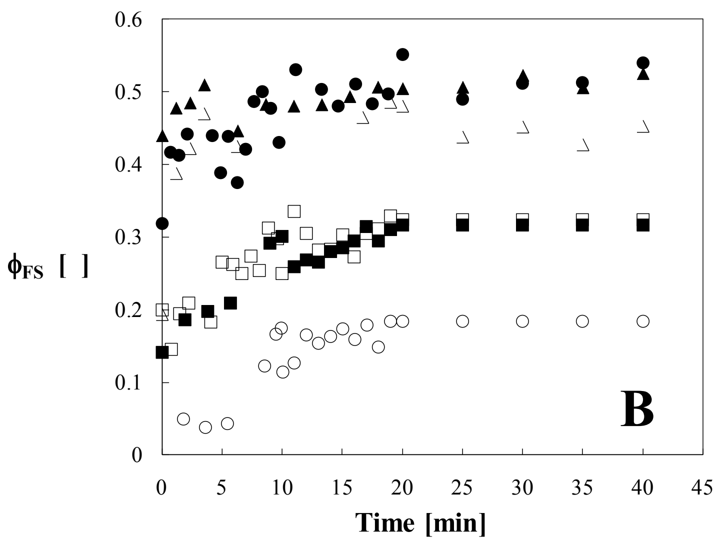

0.6
0.5
0.4
0.3
0.2
0.1
0
ϕ_{FS} [ ]
0
5
10
15
20
25
30
35
40
45
Time [min]
B

Fig. 7

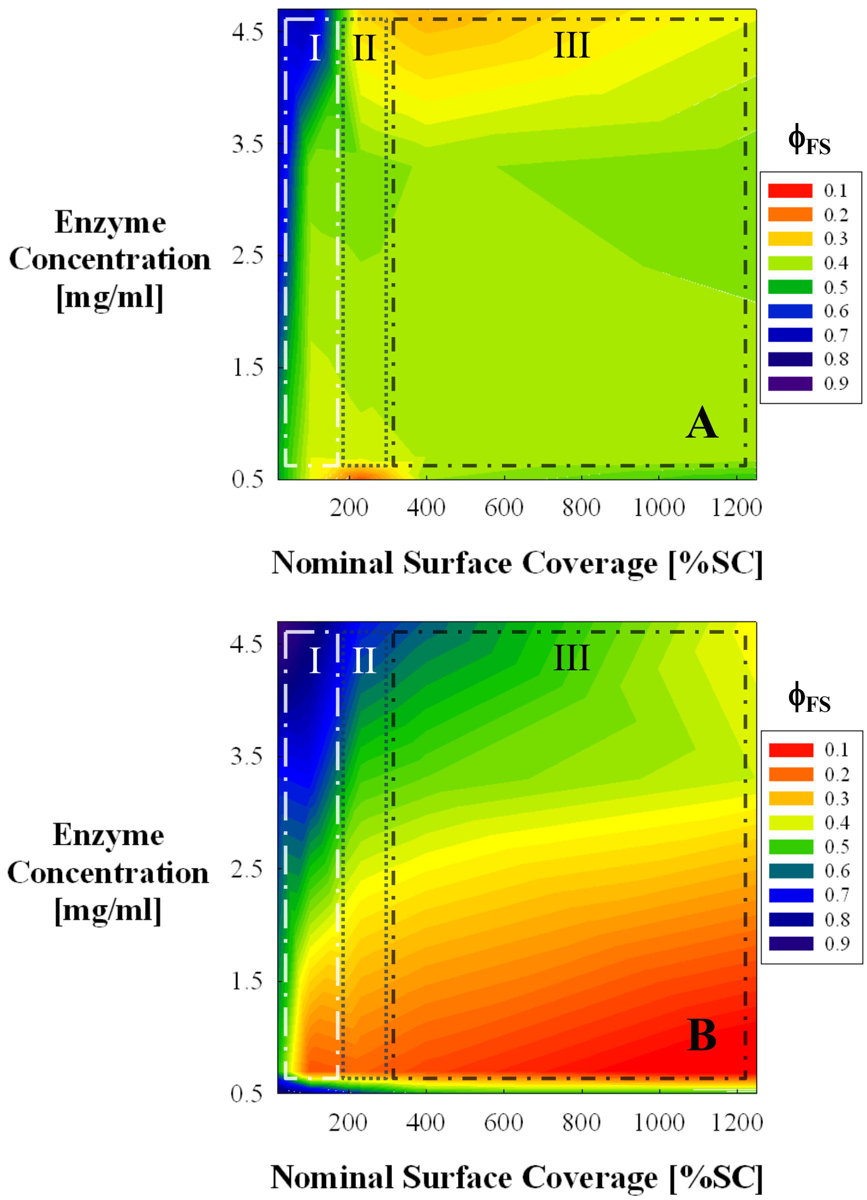
Enzyme Concentration [mg/ml]
4.5
3.5
2.5
1.5
0.5
200
400
600
800
1000
1200
Nominal Surface Coverage [%SC]
I
II
III
A
ϕ_{FS}
0.1
0.2
0.3
0.4
0.5
0.6
0.7
0.8
0.9
B

Fig. S1

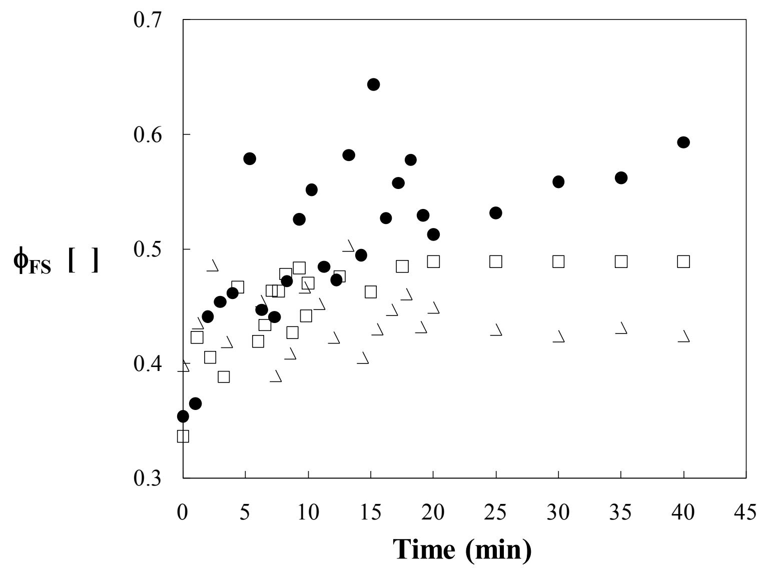

Fig. S2

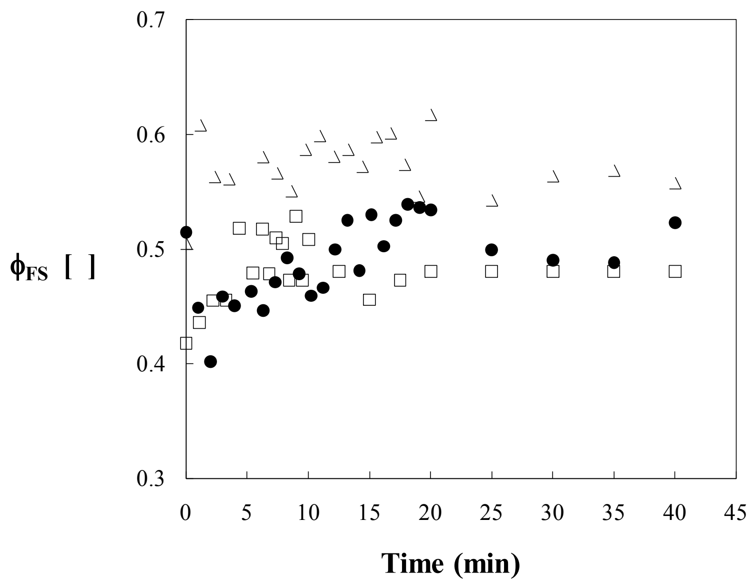

Fig. S3

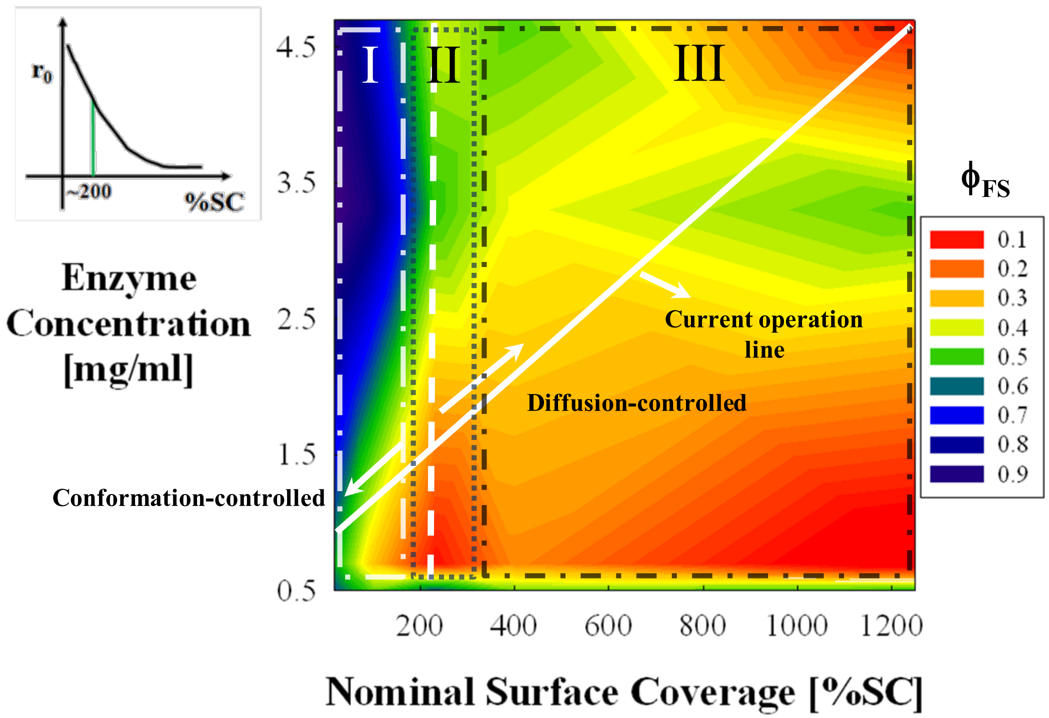

r_0
~200
%SC
Enzyme Concentration [mg/ml]
4.5
3.5
2.5
1.5
0.5
I
II
III
Current operation line
Diffusion-controlled
Conformation-controlled
200
400
600
800
1000
1200
Nominal Surface Coverage [%SC]
ϕ_{FS}
0.1
0.2
0.3
0.4
0.5
0.6
0.7
0.8
0.9

Fig. S4

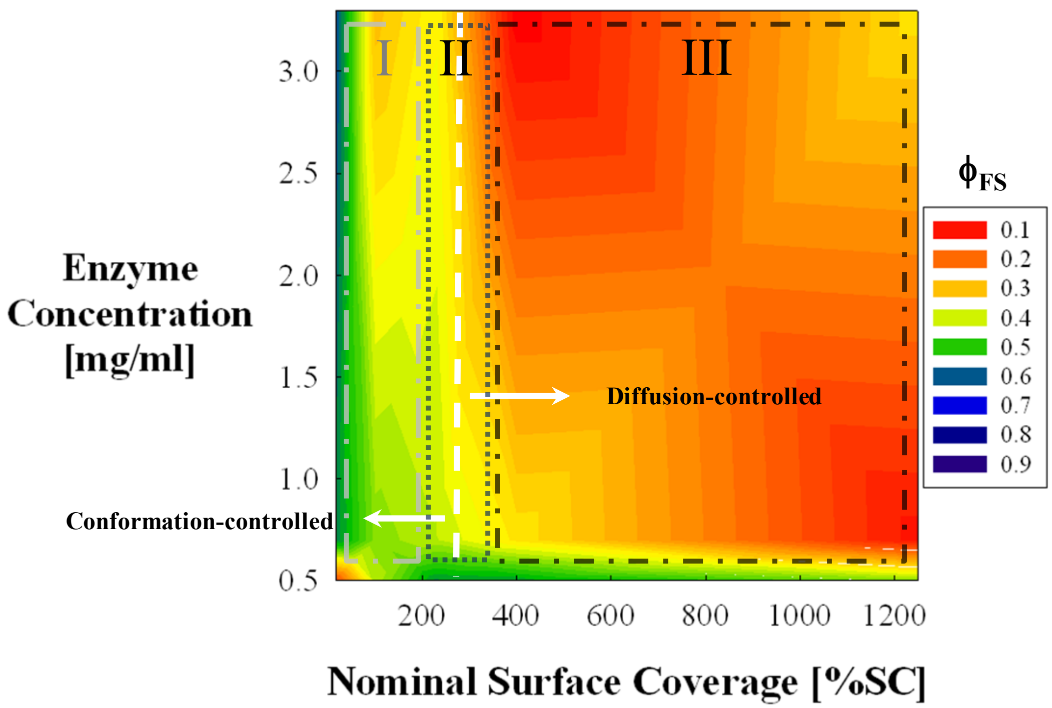

I
II
III
Enzyme Concentration [mg/ml]
3.0
2.5
2.0
1.5
1.0
0.5
200
400
600
800
1000
1200
Nominal Surface Coverage [%SC]
Diffusion-controlled
Conformation-controlled
ϕ_{FS}
0.1
0.2
0.3
0.4
0.5
0.6
0.7
0.8
0.9